THE UNIVERSITY OF MICHIGAN
COLLEGE OF ENGINEERING
Aeronomy Program

Aeronomy Program Report No. 1

STELLAR SPECTRA AND ATMOSPHERIC COMPOSITION

P. B. Hays
R. G. Roble

ORA Projects 06647 and 08953

under contract with:

NATIONAL AERONAUTICS AND SPACE ADMINISTRATION
CONTRACT NO. NAS r-54(08)
WASHINGTON, D.C.

and

NATIONAL SCIENCE FOUNDATION
GRANT NO. GA-1025
WASHINGTON, D.C.

administered through:

OFFICE OF RESEARCH ADMINISTRATION ANN ARBOR

November 1967

Abstract

The distortions to the image and spectrum of a star being observed during occultation from a satellite are discussed. The primary distortions are shown to be due to refractive dispersion, small and large particle scattering, and absorption by various atmospheric gases. Representative stellar spectra in both the visible and ultraviolet are presented, and various features relating to specific atmospheric constituents are discussed. The possibility of recovering information concerning atmospheric composition from stellar spectra is considered and several distinct processes are used for illustration. The recovery of airglow emission profiles from satellite observations of the airglow at the limb of a planet is shown to be similar to the recovery of atmospheric structure from stellar occultation data.

1. Introduction

The Earth's atmosphere has for centuries been the cause of considerable inconvenience to the astronomer, distorting and spectrally filtering the image of stars viewed from ground based observatories. The gases surrounding the Earth act as a complex prism, refracting, absorbing, and dispersing light which originates from extra-terrestrial objects in a manner analogous to a conventional spectroscope. However, these effects which are so troublesome to astronomers can be of considerable interest to the geophysicists in the study of atmospheric structure and composition. In particular, if optical observations of extra-terrestrial light sources and airglow background are made during occultation from a satellite, such information offers intriguing possibilities for increasing our knowledge of the atmospheres of the Earth and planets.

The basic physical processes responsible for distorting stellar images are refraction, scattering, and absorption of light as it passes through the atmosphere. Since these effects are most pronounced when the object is viewed horizontally, we will consider the situation in which a stellar image is examined from a satellite observation platform during the period of occultation. During occultation all of these distorting effects become progressively more pronounced as the star approaches the horizon and the light traverses the more dense portions of the atmosphere. As the star approaches the horizon, refraction distorts the ideal point image into a linear spectrum, as well as causing an apparent change in the astronomical position of the star. Rayleigh and Mie scattering of the transmitted

starlight is most effective in dense portions of the atmosphere, and at short wavelengths there are strong attenuations resulting from excitation, photo-dissociation, and ionization of the various constituent gases. These attenuation processes are all strongly dependent on the wavelength of the light being observed; in particular, the photo-absorption processes have definite thresholds and strong absorptions associated with specific atmospheric gases.

2. Refraction

The theory describing the occultation of a star by a planet with an atmosphere observed from a ground based observatory was first given by Pannekoek [1903]. However, the application of the theory had to wait for the combination of modern photometric techniques and the planetary occultation of a sufficiently bright star. Baum and Code [1953] were the first to apply photometric techniques to the method and measured the occultation of Sigma Arietis by Jupiter. The extinction resulting in this occultation was primarily due to refractive dispersion which dominates all other effects and becomes effective while the occulted star light is still passing through the upper atmosphere of the planet. Thus Baum and Code, using the occultation technique, were able to arrive at a scale height for the upper atmosphere of Jupiter. Weisberg [1962] considered this technique as a method of sounding an atmosphere by measuring the extinction due to the refractive dispersion of occulting stars observed from a satellite. Recently, Jones, et al [1962], have discussed a technique for measuring the structure of the earth's stratosphere which utilizes a continuous recording of the angular refraction of star light from a satellite. This method of

extracting information about the atmosphere from optical observations of the refracted star image is based upon the fact that a knowledge of the refraction angle as a function of the position of the star above the horizon is entirely sufficient to determine the index of refraction as a function of height above the planetary surface. Since one knows the composition of the Earth's lower atmosphere, the density is obtained directly from the scan of the stellar refraction angle.

Mathematically, this process is entirely analogous to the investigation of the propagation of seismic waves and the determination of the structure of the solid Earth as discussed by Bateman [1910], which has received considerable attention from the geologist. The refraction angle of a star, when viewed from outside a spherically stratified atmosphere, obeys the equation

$$R(\mu_o r_o) = 2\mu_o r_o \int_{\mu_o r_o}^{\infty} \frac{\frac{d \log \mu}{d(\mu r)}\, d(\mu r)}{\sqrt{(\mu r)^2 - (\mu_o r_o)^2}} \tag{1}$$

where μ is the index of refraction, r is the radial distance from the center of the planet to the ray path, and the subscript o refers to the point of closest approach to the planet, the tangent point. The geometry of refraction is illustrated in Fig. 1. Rays of starlight, as well as seismic rays, are brachistochrones and both traverse spherically stratified media; consequently they obey Snell's law

$$\mu_o r_o = \mu r \sin Z = \text{constant}. \tag{2}$$

Here Z is the zenith angle of the ray measured from the radius vector.

Thus, since the measurement is carried out from a satellite at $r = r_s$, $\mu_s = 1.0$ and knowing Z_s at the satellite, the refraction angle is known in terms of the parameter

$$\mu_o r_o = r_s \sin Z_s \tag{3}$$

The refraction equation (1) is an Abel's integral equation and allows the simple inversion

$$\mu = \text{EXP}\left\{ -\frac{1}{\pi} \int_{\mu r}^{\infty} \frac{R(\mu_o r_o)\, d(\mu_o r_o)}{\sqrt{\mu_o^2 r_o^2 - \mu^2 r^2}} \right\} \tag{4}$$

yielding the index of refraction as a function of the distance above the surface of the planet. The use of Gladstone and Dale's [The International Dictionary of Physics and Electronics, 1956] law allows one to obtain the atmospheric density directly from the index of refraction

$$\mu = 1 + k(\lambda)\rho \tag{5}$$

where $k(\lambda) = (77.6 + \frac{0.584}{\lambda^2}) R \times 10^{-6}$ [Handbook of Geophysics, 1960], R is the gas constant of air and ρ is the mass density of the atmosphere. The above relations apply to monochromatic light; the result of examining a rather broad spectral band complicates the process but does not fundamentally affect the result. The practical analysis of the refraction technique has been discussed by Fischbach [1965] and a more detailed analysis of the scheme will be given in future papers. Here, we will analyze the shape and structure of the broadband image as it passes through the atmosphere and discuss the resulting distortions as they are related to the atmosphere.

Before considering the distortion and attenuation of the stellar image,

it is useful to record a simple approximation to the refraction angle in an exponential atmosphere

$$\rho = \rho_o \, \mathrm{EXP}\left[-(r-r_o)/H\right]. \tag{6}$$

Here H is the scale height and ρ_o is the density at the reference level. Making use of equation (1), Gladstone and Dale's law (5) and neglecting the square of the quantity $(\mu-1)$ compared to 1.0

$$R(r_o, \lambda) = k(\lambda) \cdot \rho \ (r_o) \sqrt{\frac{2\pi r_o}{H}} \tag{7}$$

The prediction of refraction angles from equation (7) is good to a few percent and consequently will yield results of sufficient accuracy for our purposes when considering the dispersion and attenuation which result from refraction. For comparison, the refraction angle as a function of tangent ray height for light of wavelength $\lambda = 7000$ Å is tabulated in Table 1 for the CIRA 1965 atmosphere using equation (1), the simple exponential approximation based on local density and scale height, and an exponential approximation based on a constant scale height. The exponential approximations are obviously suitable for most computations.

3. Dispersion and Attenuation of Visible Light

The dispersion and attenuation of the short wavelength radiation coming from an occulting star can be conveniently discussed by separating the spectral region into the visible and ultra-violet. Here we include the near ultra-violet and near infrared in the visible spectrum and all shorter wavelengths in the ultra-violet. The visible spectral region is distorted primarily by the dense portions of the Earth's atmosphere, the troposphere and stratosphere, where scattering, refractive attenuation and distortion, and ozone absorption in the Chappuis band are predominant features.

In this region of the atmosphere, the ultra-violet is almost entirely absorbed. The ultra-violet region of the spectrum is of interest for rays of light which penetrate the more tenuous fringes of the atmosphere, the mesosphere and thermosphere of the Earth, where the visible spectrum is transmitted without distortion. These shorter wavelengths have sufficient energy to cause dissociation and ionization of various constituent gases; as a consequence, the dissociation and ionization spectra of a number of atmospheric constituents appear in the transmitted stellar spectrum. The following discussion will be divided according to these two physically distinct spectral and atmospheric regions. Although the atmosphere of the Earth will be used as the primary example, the results obtained here are nearly all directly applicable to other planetary atmospheres as well.

When light passes through a large air mass, as it must when an occulting star is viewed near the horizon, the most significant processes affecting the transmitted light are those which have small attenuation cross-sections or which are caused by very minor constituents. Any major attenuation process causes the atmosphere to be opaque in the affected spectral region. In the Earth's atmosphere, Rayleigh or molecular scattering, Mie scattering, as well as refractive dispersion and ozone absorption, provide the primary loss processes for visible light passing through the lower dense regions. Unfortunately, in the denser regions of the atmosphere one cannot consider these effects separately. Refraction causes the individual rays of light to follow curved paths and thus is intimately connected with the total number of particles along a given ray. This is particularly significant since the wavelength is dependent on the index of refraction, which causes rays

from different spectral regions to follow separate paths through the atmosphere.

In general, a ray of light of wavelength λ suffers attenuation

$$\frac{I(\lambda, r_o)}{I\infty(\lambda)} = \text{EXP}\left\{ -\sum_i \int_{-\infty}^{\infty} \sigma_i N_i(s)\, ds \right\} \psi(\lambda, r_o) \qquad (8)$$

where $I\infty(\lambda)$ is the intensity in the absence of attenuation, $I(\lambda, r_o)$ is the intensity of the ray after passing through the atmosphere with tangent height r_o, σ_i the cross-section for scattering or absorption and N_i the number density of i^{th} species, and $\psi(\lambda, r_o)$ is the change in intensity due to refractive dispersion of the light. Here the integration is carried out along the path of the refracted light and ds is the element of length along this path. (See Figure 1). The major result of refraction on the path of a given ray of light is to change the height of the point of tangency of the ray. Since the curvature is small, it is usually sufficient to treat the ray as though it were a straight line passing tangent to the planet at a height r_o which is determined by refraction.

The tangent height of a given ray of wavelength λ when viewed from outside the atmosphere is determined by the angular position and height of the observer and by the wavelength of the ray of light. All rays observed at the position r_s, θ_s of the satellite observer must intersect at that point. That is, from the geometry illustrated in Figure 1, the angle Θ_s is a constant for all rays, where

$$\Theta_s = \pi + R(\lambda, r_o) - \text{SIN}^{-1}\left\{ \frac{r_o + b}{r_s} \cdot \text{COS}^{-1}\left(\frac{R(\lambda, r_o)}{2} \right) \right\} \qquad (9)$$

By using Snell's law (3), the Gladstone and Dale law (5), and expressing b in terms of μ_o, r_o, and R one finds

$$\Theta_s = \pi + R(\lambda, r_o) - \text{SIN}^{-1}\left\{\frac{r_o(1+k(\lambda)\rho_o}{r_s}\right\} \tag{10}$$

Here ρ_o and $k(\lambda)$ refer to the major constituents which determine the angular refraction. In theory, this equation for r_o could be solved in terms of λ, Θ_s and r_s, but this is impractical and the process can be simplified by expanding the equation about a specific point r_o^* which is the tangent ray height for a ray with wavelength λ^*. This is possible whenever $k(\lambda)$ is a slowly varying function of wavelength. This leads to the result that

$$r_o(\lambda) = r_o^* + \Delta r_o(\lambda) \tag{11}$$

where

$$\Delta r_o(\lambda) = \frac{\left(\frac{\partial \Theta_s}{\partial k}\right)_{r_o}}{\left(\frac{\partial \Theta_s}{\partial r_o}\right)_k}\left(k(\lambda) - k(\lambda^*)\right) \tag{12}$$

For an isothermal atmosphere

$$r_o(\lambda) = r_o^* + \left\{\frac{\rho_o^*\sqrt{\frac{2\pi r_o^*}{H}} - \frac{r_o^*\rho_o^*}{\sqrt{r_s^2 - \mu_o^{*2} r_o^{*2}}}}{\frac{2\pi(\mu_o^* - 1)}{H}\left[\frac{-H+2r_o^*}{\sqrt{8\pi H r_o^*}}\right] + \frac{\mu_o^* - \frac{r_o^*}{H}(\mu_o^* - 1)}{\sqrt{r_s^2 - r_o^{*2}\mu_o^{*2}}}}\right\}\left|k(\lambda) - k(\lambda^*)\right| \tag{13}$$

Thus one observes that for short wavelengths, where the index of refraction is larger, the tangent ray height is higher than for longer wavelengths. This effect is illustrated in Figure 2 where Δr_o is presented as a function of r_o^* and λ for $\lambda^* = 7000\,\mathring{A}$ for an observer 500 km above

the Earth. Using these results, we can now discuss the effects of scattering and absorption on the intensity of transmitted star light.

3.1 Refractive Dispersion

The distortion of the planar wave front, due to refraction, as the light passes through the atmosphere causes changes in intensity of the transmitted radiations. This change in intensity is due to the variation in cross-sectional area of a bundle of light rays as it passes through the atmosphere. From the geometry in Figure 1, we find the intensity reduction to be

$$\psi(\lambda, r_o) = \frac{p}{\left| r_s \mathrm{SIN}\Theta_s \right|} \cdot \frac{\mathrm{COS}\, R}{\left| 1+\frac{\partial}{\partial r_o}\left[\mathrm{TAN}\, R(r_s \mathrm{COS}\Theta_s - p\, \mathrm{SIN}\, \frac{R}{2})\right]\right|} \tag{14}$$

or neglecting terms of the order R^2

$$\psi(\lambda, r_o) = \frac{\mu_o r_o}{\left| r_s \mathrm{SIN}\Theta_s \right|} \cdot \frac{1}{\left| 1+r_s \mathrm{COS}\Theta_s \cdot \frac{\partial R}{\partial r_o} \right|} \tag{15}$$

which for an observer near the Earth or planet becomes approximately

$$\psi(\lambda, r_o) = \frac{1}{1 + r_s\, \mathrm{COS}\, \Theta_s \cdot \frac{\partial R}{\partial r_o}} \tag{16}$$

Since $r_s\, \mathrm{COS}\, \Theta_s$ and $\frac{\partial R}{\partial r_o}$ are in general negative, the net result of differential refraction in the immediate vicinity of a planet is a reduction in intensity. The transmission function for differential refraction in the Earth's atmosphere is illustrated in Figure 3 for an observer 500 km above the Earth's surface. Notice that the variation with wavelength is very slight and for practical purposes may generally be neglected. The isothermal approximation for the refractive attenuation is

$$\psi(\lambda, r_o) = \frac{1}{\left[1 - \frac{r_s \cos\Theta_s}{H}\sqrt{\frac{2\pi r_o}{H}}\, k(\lambda)\rho_o\right]} \tag{17}$$

This function is normally sufficiently accurate to predict the attenuation caused by refraction and certainly can be used to make any wavelength correction.

3.2 Molecular Scattering

The cross-section for Rayleigh or molecular scattering is

$$\sigma_i = \frac{128\pi^5}{3\lambda^4}\,\alpha_i^2 \tag{18}$$

where α_i is the polarizability of the i^{th} species of scatterer at wavelength λ. Writing this in terms of the index of refraction for air, Allen [1963],

$$\sigma_R = \frac{32\pi^3 k^2(\lambda) M}{3\lambda^4} \tag{19}$$

where M is the mass of a hypothetical air molecule. Consequently, the attenuation of a ray of star light with wavelength λ in a spherically stratified atmosphere due to Rayleigh scattering is

$$T_R = \left[\frac{I(\lambda)}{I\infty(\lambda)}\right]_R = \mathrm{EXP}\left\{-\frac{64\pi^3 k^2(\lambda) M^2}{3\lambda^4}\int_{r_o(\lambda)}^{\infty}\frac{N(r)\, r\, dr}{\sqrt{r^2 - r_o^2(\lambda)}}\right\} \tag{20}$$

where T is known as the transmission function. This expression can be approximated for an exponential atmosphere as

$$T_R = \mathrm{EXP}\left\{-\frac{32\pi^3}{3\lambda^4}\, k^2(\lambda) M^2 N_o(\lambda)\sqrt{2Hr_o(\lambda)}\right\} \tag{21}$$

Here r_o, N_o are evaluated at the height $r_o(\lambda)$. We see from this expression that the error due to neglecting the change in height of various wavelengths

is rather small of the order $\Delta r_o / H$ which is in general less than 10% for the visible and near ultra-violet. This is due to the fact that the main atmospheric constituents change relatively slowly with height, but the situation can be of greater importance for particles which show greater gradients such as small particle Mie scatterers. The attenuation due to Rayleigh scattering is one of the factors that can be predicted quite accurately, and consequently does not enter into consideration as an unknown to be determined, but is a factor that must be removed from any experimental results before an analysis of the transmitted spectra can be made. The transmission function for Rayleigh scattering is shown in Figure 4 as a function of tangent ray height and wavelength in an exponential atmosphere.

3.3 Mie Scattering

The distribution of small particle scatterers such as large aerosols and Aitkin particles in the troposphere and stratosphere is not well known. Even the assumption of spherical stratification should be viewed with suspicion. However, Junge [1963] and Chagnon and Junge [1961] have presented the results of several experimental determinations of particle size distribution and profiles of the distribution of particles with height. Utilizing the empirical power law size distribution derived by Junge [1963] and incorporating the scattering coefficient approximation given by Van-De Hulst [1962], a mean cross-section for Mie scattering is obtained

$$\sigma_M(\lambda) = \pi\left(\frac{C}{2.3}\right)\left(\frac{\lambda}{2\pi}\right)^{2-\beta} \int_{X_1}^{X_2} \left(2 + \frac{4}{\xi}\,\mathrm{SIN}\xi + \frac{4}{\xi^2}\,(1-\mathrm{COS}\,\xi)\right) \cdot X^{(1-\rho)}\, dx \qquad (22)$$

where $\xi = 2/M' - 1/x$, M' being the index of refraction of the particles,

$x = 2\pi\, r/\lambda$ where r is the particle radius, and c and β are constants used by Junge to characterize particle size distribution. Here X_1 and X_2 are the limits on the distribution of particle radii.

The transmission function resulting from a spherically stratified distribution of these particles can be approximated by the relation

$$T_M = \left[\frac{I(\lambda)}{I\infty(\lambda)}\right]_M = \mathrm{EXP}\left\{-2\sigma_M(\lambda)\int_{r_o(\lambda)}^{\infty}\frac{N_M(r)\, r\, dr}{\sqrt{r^2 - r_o^2(\lambda)}}\right\} \qquad (23)$$

where N_M is the total number density of Mie scatterers. Once again the curvature due to refraction has been included only through the tangent ray height.

To illustrate the region of major influence of aerosol scattering, the results of calculations of the Mie particle transmission function for the experimental distributions given by Junge [1963] are shown in Figure 5. These results illustrate the variation of intensity with wavelength and tangent ray height due to Mie scattering alone. As expected, the loss due to these larger particles is not strongly dependent on wavelength.

3.4 Ozone Absorption

In the visible region of the spectrum, the Chappuis band of Ozone is the primary cause of direct-photo absorption. The photo absorption cross-section as a function of wavelength is shown in Figure 6. Although the distribution of ozone with height has been the subject of considerable study, it is not well known at present. There are as yet unexplained seasonal and latitudinal variations according to Hunt [1966] and Roney [1965] which seem to depend upon stratospheric circulation, but which may be related to water-vapor distributions.

For the purpose of illustration, we have taken as a typical ozone profile that given by Green [1964] in the form

$$N_{o_3}(r) = \frac{W_p}{h} \frac{\text{EXP}\left[(r-r_p)/h\right]}{\left\{1+\text{EXP}\left[(r-r_p)/h\right]\right\}} \tag{24}$$

where $W_p = .582 \times 10^{+14}$, $h = 4.63$, and $r_p = r_e + 23.23$ km all adjusted to give a reasonable standard ozone profile.

Since the lateral variations of ozone are gradual, spherical stratification can be assumed. Therefore, the transmission function due to ozone can again be given by the simple expression

$$T_{o_3} = \left[\frac{I(\lambda)}{I_\infty(\lambda)}\right]_{o_3} = \text{EXP}\left\{-2\sigma_{o_3}(\lambda) \int_{r_o(\lambda)}^{\infty} \frac{N_{o_3}(r)\, r\, dr}{\sqrt{r^2 - r_o^2(\lambda)}}\right\} \tag{25}$$

which is shown in Figure 7 for the model ozone profile described above. The strong attenuation in the center of the Chappuis band and the tendency for the attenuation to remain constant below the ozone peak is clearly illustrated. However, these results represent at best only a mean condition.

3.5 Minor Contributions

There are several other minor contributions to attenuation in the lower atmosphere. Water vapor occurs primarily below the tropopause where clouds will generally interfere with transmitted light and will cause the apparent horizon to be above the region where water vapor itself is important. Atmospheric turbulence can contribute to the reduction in intensity and give rise to intensity fluctuations, but this effect is probably confined to the troposphere and should not cause serious attenuation above the cloud-top level. The result of any turbulence would be a refractive

type of dispersion due to small scale irregularities in the index of refraction. Molecular oxygen has several minor absorption bands in the visible; however, these are narrow and should be of lesser importance than the factors previously discussed. The minor constituents CO_2, N_2O, and CH_4 are of very little consequence in the visible region of the spectrum and may be ignored. Intense resonant line scattering such as the sodium doublet occupy such narrow spectral regions that they can also be neglected.

4. Visible Spectra

The results obtained thus far allow us to discuss the visible spectrum of occulting stars for a mean atmosphere. We will adopt the empirical expression given by Allen [1963] to simulate the visible stellar spectrum above the atmosphere

$$I_\infty(\lambda) = \text{EXP}\left[-(0.921M_v + 19.388)\right]\left(\frac{\lambda_o}{\lambda}\right)^5 \frac{\left[\text{EXP}\left(\frac{1.438\text{x}10^7}{\lambda_o T}\right) - 1\right]}{\left[\text{EXP}\left(\frac{1.438\text{x}10^7}{\lambda T}\right) - 1\right]} \text{x}10^{-7} \frac{\text{WATTS}}{\text{CM}^2\text{-}\mathring{\text{A}}} \tag{26}$$

where $\lambda_o = 5500\ \mathring{\text{A}}$, M_v is the visual magnitude, and T the effective blackbody temperature of the star. For the purpose of illustration, we have chosen a type G0 star of visual magnitude + 1 with an effective blackbody temperature of $6000^\circ K$. When the attenuating factors considered in the previous sections are combined with the assumed spectral distribution of the star and due consideration is given to the fact that each wavelength corresponds to its individual tangent ray height around the base ray, then the transmission spectrum of the star may be calculated. The spectral

distribution as a function of wavelength and tangent ray height (with reference wavelength at $\lambda^* = 7000$ Å) is given in Figure 8. Above 40 km there is little attenuation, but below that altitude the Chappuis band of ozone is a prominent feature slightly above 6000 Å. As the altitude decreases, Rayleigh scattering intensifies in the shorter wavelength region causing the relative maximum around 5000 Å to decrease more rapidly than that at longer wavelengths. This phenomenon is of course responsible for the red sun we see at sunset. There is a general decay of the entire spectrum associated with refractive dispersion, Rayleigh scattering, and at lower altitude Mie scattering.

4.1 Shape of Stellar Images

We have also considered the shape of an image seen from an orbiting observatory. This question is of interest particularly in view of the suggestion that refraction angles be used directly to recover atmospheric structure. In Figure 9 we have combined the spectral attenuation profile and the angular distribution of light between 3000 Å and 11,000 Å observed from a satellite at a height of 500 km, to give image contours. The main features present in the spectra are displayed here where the atmosphere itself takes on the role of the prism in a conventional spectroscope. It can be seen that the initial point source of the star above the atmosphere is spread out into a line spectrum along the density gradient in the Earth's atmosphere. Again the base ray is $\lambda_o^* = 7000$ Å, and it is shown (Figure 9) that along with the general energy decay due to the attenuating factors there is a broadening of the image as one proceeds lower in the atmosphere. The broadening is most

pronounced in the blue end of the spectrum. The most prominent feature is the strong ozone absorption valley near 6000 Å.

To determine the stellar shape which would be distributed over a typical photocathode surface, we have included in a second spectrum the spectral characteristics of a S-20 photocathode (Figure 10), which has a good response over most of the region considered. The resulting images illustrate the general decay with tangent ray height due to the attenuating factors and show a general shift in the image centroid during occultation. This shift is quite significant and surely would have to be removed if star tracking of a few arc seconds were required.

5. Absorption of Ultra-violet Light

Although the less dense regions of the atmosphere have little influence on visible light, they do strongly influence the ultra-violet portion of the spectrum. Of the factors previously discussed, only Rayleigh scattering and ozone absorption are influential at higher altitudes and shorter wavelengths; Rayleigh scattering due to the increase of the cross-section at shorter wavelengths, and ozone due to the existence of the strong Hartley-Continuum and Huggins absorption band in the ultraviolet. In addition to these features, the dissociation and ionization spectra of molecular oxygen, atomic oxygen and other atmospheric gases become important. Here only the spectral region between 1200 Å and 3500 Å, a region in which the influence of molecular oxygen and ozone predominates, will be discussed. The photoabsorption cross-sections for these molecules are presented in Figure 6 obtained from Watanabe [1958] and Ditchburn and Young [1962]. The data in the Schumann-Runge band system of molecular

oxygen for 1750 - 2000 Å are poorly defined and consequently will not be used in the following discussion.

5.1 Rayleigh Scattering

Fortunately, Rayleigh scattering in the Earth's atmosphere is important only up to about 80 km, and thus can be predicted without great uncertainty. The transmission function for Rayleigh scattering is presented in Figure 4 as discussed in section 3.2. Above 80 km its influence is negligible as an attenuating factor in the spectral region discussed here.

5.2 Ozone

Ozone is the dominant factor in determining the ultra-violet spectra between 2000 Å and 3500 Å for rays of starlight passing through the mesosphere. However, the uncertainty in the mesospheric ozone profile is large. Large diurnal and seasonal variations occur in this region, but no adequate theoretical treatment of the ozone photo-chemistry is as yet available. The influence of small amounts of water vapor and associated hydrogen compounds appears to be very important, and above 80 km the complex ozone-atomic oxygen transport and photo-chemical processes cannot be adequately treated due to the lack of fundamental information concerning transport processes as well as a lack of accurate data on the rate coefficients for various important photo-chemical reactions.

To illustrate the variability of the influence of ozone on stellar spectra, four examples are presented in Figures 11 - 14 showing the extreme diurnal variation of the ozone transmission function for theoretically predicted ozone profiles, with one pair for a pure oxygen atmosphere [London, 1967] and a second pair for a moist atmosphere [Hunt, 1966].

The effects of Rayleigh scattering and the Hertzberg system of molecular oxygen is included in these spectra, but the contributions are minor and predictable in the mesosphere.

5.3 Molecular Oxygen

Molecular oxygen, like ozone, is the subject of some uncertainty, but in contrast to ozone the uncertainty is primarily in the thermosphere. In this case, the variability is associated with the complex dissociation, diffusion, and recombination processes which occur near the "turbopause" region [Colegrove, et al, 1966]. Actually, molecular oxygen, ozone, and atomic oxygen are each individual aspects of a single phenomenon. However, molecular oxygen does not exhibit the large diurnal variation of ozone and in this sense, its behavior is less complex.

In the upper thermosphere above 150 km, diffusive equilibrum prevails allowing the neutral gas temperature to be related to the molecular oxygen profile. The transmission function for molecular oxygen absorption between 1200 $\mathring{A}$ and 1700 $\mathring{A}$ for the average atmosphere of Colegrove, et al, is shown in Figure 15.

6. Ultra-violet Spectra

Stellar class O and B stars with a high effective temperature have a blackbody emission spectrum peaking near the ultra-violet region of interest. To show a typical transmission spectra, we have chosen the star γCih Cas, a class BO star, with an effective blackbody temperature of 21,000^{o}K and a visual magnitude of 2.15 [Allen, 1963] and have calculated the transmission spectra at various altitudes during occultation. This transmission spectra is shown in Figure 16 where the initial blackbody

distribution is seen to be altered and attenuated as a result of molecular oxygen absorption in the region 100-250 km and by the combined effects of molecular oxygen absorption, Rayleigh scattering, and ozone absorption in the region 40-100 km. The Hunt nighttime ozone profile was used in these calculations.

7. Vertical Profiles of Absorbing Species from Spectral Data

The stellar spectra discussed in the previous sections contain in their detail an enormous amount of information about the atmosphere. An interesting possibility exists for extracting this information, that is, determining vertical profiles of the attenuating species directly from measurements of the transmitted spectra. Consider the transmission function for a particular absorbing species

$$T_i(r_o,\lambda) = \mathrm{EXP}\left\{-2\sigma_i(\lambda)\int_{r_o}^{\infty}\frac{N_i(r)\,r\,dr}{\sqrt{r^2-r_o^2}}\right\} \tag{27}$$

which can be written as the integral equation

$$\int_{r_o}^{\infty}\frac{N_i(r)\,r\,dr}{\sqrt{r^2-r_o^2}} = \log\left(\frac{1}{T_i(r_o,\lambda)}\right)^{2\sigma_i(\lambda)} \tag{28}$$

We note that equation (28) is an Abel integral equation of outwardly the same nature as the refraction equation (1) and consequently can be inverted to yield the number density $N_i(r)$ in the following form

$$N_i(r) = \frac{1}{2\pi\sigma_i(\lambda)}\frac{d}{dr}\left\{\int_{r}^{\infty}\frac{r}{r_o}\frac{\log\left[T_i(r_o,\lambda)\right]dr_o}{\sqrt{r_o^2-r^2}}\right\} \tag{29}$$

A discussion of a simple numerical inversion technique is presented in

Appendix I.

Thus, if we were to measure the intensity of the stellar spectra even at relatively isolated wavelengths, for a series of tangent ray heights as a star is occulted, it would be possible to invert the data and retrieve vertical profiles of the number density of the absorbing gases. The spectral resolution required depends upon the altitude range over which the profile would be measured and, of course, on the number of unknown absorbers that must be separated. The process of inversion would in general be iterative and subject to some error due to the lack of knowledge concerning the cross-sections for the various absorption processes. As a practical note, it is interesting to point out that only the relative change of intensity of the starlight is required if there are no intense emission lines in the stellar spectral region of interest and that if a region where the cross-section is relatively constant is used, even emission lines become unimportant.

Consider again the visible and ultra-violet spectral regions. In the lower atmosphere where ozone, scattering, and refractive dispersion affect the visible spectrum, one can recover the ozone and Mie scatter density profiles after removing the effects of Rayleigh scattering and refractive dispersion which are relatively predictable. This has been attempted previously using sunlight reflected by an occulting satellite. Venkateswaran, et al [1961] sought to recover the ozone density profile near sunset in this manner; however, the sun subtends such a large angle at the earth that the broadening badly degrades the results. The technique used by Venkateswaran, et al was to obtain photometric data in two narrow spectral

regions, one lying in the center of the Chappuis absorption band and the other nearby, but away from, the peak absorption. Thus, the effects of scattering and refractive dispersion are in principle monitored and removed by subtraction of the data in the two spectral regions. This technique is useful and could be extended by using several isolated bands chosen to monitor the important scattering and attenuation effects, but starlight would be a preferable probe.

The stellar ultra-violet spectrum for light transmitted through the upper mesosphere and thermosphere is affected primarily by ozone and molecular oxygen. Not only are these effects predominately restricted to two spectral regions, but also, from the previous discussion, the altitudes for which there is uncertainty in the number density of each species are distinct. The obvious implication is that between 100 and approximately 250 km, the molecular oxygen density can be recovered using spectral data from a region centered at about 1450 $\mathring{A}$. Possibly a single broadband photometer would suffice since the cross-section is relatively constant near 1450 $\mathring{A}$ and thus variations in the undistorted stellar spectrum would not be important. The Shumann-Runge Band system should, of course, be avoided. At lower altitudes, from about 50-100 km, there are two spectral regions of interest in determining the high level ozone profile, one near 2100 $\mathring{A}$ and a second near 2500 $\mathring{A}$. Again photometric measurements of relatively low resolution would cover the desired altitude range and be insensitive to the slope of the undistorted stellar spectrum. The effects of Rayleigh scattering and molecular oxygen would have to be removed at low altitudes, but this should not be serious since both the total number

density and the molecular oxygen density are predictable below 100 km.

8. Airglow and Scattered Light

The general inversion technique discussed here can be applied to a very large class of atmospheric measurements.

The measured intensity of the light emitted or scattered from any spherically stratified source of emission in the atmosphere is given by the relation

$$F_\lambda (r_o) = \frac{A\Omega}{2\pi} \int_{r_o}^{\infty} \frac{E_\lambda (r)\, r\, dr}{\sqrt{r^2 - r_o^2}} \tag{30}$$

where F_λ is the number of photons/sec entering a telescope of aperture A and field of view Ω from a spherically stratified source of diffuse emission, with volume emission rate $E_\lambda (r)$ photon/cm^3 sec when the tangent ray height is r_o. Here the field of view is assumed to be small. The Abel inversion of this integral relation yields the emission profile

$$E_\nu (r) = -\frac{4}{\Omega A} \frac{d}{dr} \int_r^{\infty} \frac{r}{r_o} \frac{F_\nu (r_o)\, d\, r_o}{\sqrt{r_o^2 - r^2}} \tag{31}$$

This is precisely the same as the inversion for spherically distributed source of absorption. The measurement of such quantities has been carried out in several cases. Reed and Blamont [1967] have measured the $O(^1D) - O(^3P)$ 6300 Å red line emission from a satellite using a photometer with a $1/2^o$ field of view. Barth [1967], has measured the intensity of singly scattered Lyα from the Mariner 5 spacecraft during its exit from the Earth in order to obtain the terrestrial hydrogen density distribution and plans to make a similar measurement in the Cytherean atmosphere. However, one difficulty with the measurement of emissions or scattered

light is the existence of instrumental broadening due to the necessarily finite field of view of the observing instrument. The result of the finite field of view is to average the emission profile over a rather large altitude region, which is in sharp contrast to the observation of starlight where the altitude spread of the observed light is very small (i.e. of the order of the size of the telescope objective).

Appendix I Numerical Inversion Technique

The basic inversion integral used to recover atmospheric information from occultation measurements of absorption or emissions is of the form

$$x(r) = -\frac{2}{\pi}\frac{d}{dr}\int_r^\infty \frac{r}{r_o}\frac{y(r_o)\,dr_o}{\sqrt{r_o^2-r^2}} = -\frac{2}{\pi}\int_r^\infty \frac{\frac{dy(r_o)}{dr_o}\,dr_o}{\sqrt{r_o^2-r^2}} \tag{I-1}$$

inverting the integral

$$y(r_o) = \int_{r_o}^\infty \frac{r\,x(r)\,dr}{\sqrt{r^2-r_o^2}} \tag{I-2}$$

A simple scheme suitable for inverting experimental data is

$$x(r_j) = -\frac{2}{\pi}\sum_{i=j}^{M-1}\left\{\frac{y_{i+1}-y_i}{r_{i+1}-r_i}\right\}\left\{\log\frac{r_{i+1}+\sqrt{r_{i+1}^2-r_j^2}}{r_i+\sqrt{r_i^2-r_j^2}}\right\} \tag{I-3}$$

This technique has been successfully applied to emission data obtained by Reed and Blamont [1966] from the OGO-B satellite.

Acknowledgement

The work was supported by the National Aeronautics and Space Administration through Contract NAS r-54(08), and the National Science Foundation through grant GA-1025.

References

Allen, C.W., Astrophysical Quantities, 2nd Ed., The Athlone Press, University of London, 1963.

Barth, C.A., Private Communication 1967.

Bateman, H., The solution of the integral equation connecting the velocity of propagation of an earthquake wave in the interior of the earth with the times which the disturbance takes to travel to the different stations on the earth's surface, Phil. Mag., 19 (112), 576-587, 1910.

Baum, W.A., and A.D. Code, A photometric observation of the occultation of Sigma Arietis by Jupiter, Astron. J., 58 (1208), 108-112, 1953.

Chagnon, C.W. and C.E. Junge, The vertical distribution of submicron particles in the stratosphere, J. Meteorol., 18, 746-752, 1961.

Colegrove, F.D., F.S. Johnson, and W.B. Hanson, Atmospheric composition in the lower thermosphere, J. Geophys. R., 71 (9), 2227-2235, 1966.

Ditchburn, R.W. and P.A. Young, The absorption of molecular oxygen between 1850 and 2500 $\mathring{A}$, J. Atmos. Terr. Phys., 24, 127, 1962.

Fischbach, F.F., A satellite method for pressure and temperature below 24 km, Bull. Am. Meteorol. Soc., 46 (9), 528-532, 1965.

Green, A.E.S., Attenuation by ozone and the Earth's albedo in the middle ultra-violet, App. Opt., 3 (2), 203-208, 1964.

Electromagnetic wave propogation in the lower atmosphere, Handbook of Geophysics, Chapter 13, Macmillan Co., N.Y., 1960.

Hunt, B.G., Photochemistry of ozone in a moist atmosphere, J. Geophys. R., 71 (5), 1385-1397, 1966.

Jones, L. M., F. F. Fischbach, and J. W. Peterson, Satellite measurements of atmospheric structure by refraction, Planet. Space Sci., 9, 351-352, 1962.

Junge, C. E., Air Chemistry and Radioactivity, Academic Press, N. Y., International Geophysics Series, 4, 118-142, 1963.

London, J., The average distribution and time variation of ozone in the stratosphere and mesosphere, Space Research VII, North Holland Publishing, Amsterdam, 1, 172-183, 1967.

Pannekoek, A., Uber die eracheinungen, welche bei einer sternbedeckung durch einen planeten auftreten, Astron. Nach., 164 (3913), 5-10, 1903.

Reed, E. I. and J. E. Blamont, Some results concerning the principal airglow lines as measured from the OGO-II satellite, Space Research VII, North Holland Publishing, Amsterdam, 1, 337-352, 1967.

Roney, P. L., On the influence of water vapor on the distribution of stratospheric ozone, J. Atmos. Terr. Phys., 27 1177-1190, 1965.

Van De Hulst, H. C. Light Scattering by Small Particles, 2nd Ed., John Wiley, N. Y., 176, 1962.

Venkateswaran, S. V., J. G. Moore, and A. J. Krueger, Determination of the vertical distribution of ozone by satellite photometry, J. Geophys. R., 66 (6), 1751-1771, 1961.

Watanabe, K., Ultra-violet absorption process in the upper atmosphere, Advance. Geophys., Academic Press, N. Y. 5, 153, 1958.

Weisberg, H. L. The study of planetary atmosphere by stellar occultation, J. P. L. Memorandum, RM-32790JPL, 40 pp., 1962.

Table 1

REFRACTION ANGLE IN ARC SECONDS
FOR VARIOUS ATMOSPHERIC MODELS

Tangent Ray Height (KM)	CIRA 1965	Local Exponential Approximation	Isothermal based on CIRA at 10 KM
5	2412.28	2514.38	3337.89
10	1534.62	1519.77	1529.87
15	756.37	732.03	701.24
20	335.18	326.31	321.36
25	148.55	144.92	147.31
30	67.428	65.798	67.531
35	31.063	30.115	30.939
40	14.442	13.947	14.185

FIGURE LEGENDS

Figure 1. Geometry of refraction.

Figure 2. Height difference at the tangent point between base ray λ^* and ray corresponding to wavelength λ for various tangent ray heights.

Figure 3. Transmission function for refractive dispersion.

Figure 4. Transmission function for molecular scattering.

Figure 5. Transmission function for particle scattering.

Figure 6. Photoabsorption cross sections for molecular oxygen and ozone.

Figure 7. Transmission function for ozone absorption in the Chappuis band.

Figure 8. Stellar transmission spectra.

Figure 9. Angular energy dispersion for various tangent ray heights during occultation.

Figure 10. S-20 photocathode star image for various tangent ray heights during occultation.

Figure 11. Transmission function for the combined effects of molecular scattering, molecular oxygen absorption, and ozone absorption corresponding to Hunt's daytime ozone model.

Figure 12. Transmission function for the combined effects of molecular scattering, molecular oxygen absorption, and ozone absorption corresponding to Hunt's nighttime ozone model.

FIGURE LEGENDS (Concluded)

Figure 13. Transmission function for the combined effects of molecular scattering, molecular oxygen absorption, and ozone absorption corresponding to London's daytime ozone model.

Figure 14. Transmission function for the combined effects of molecular scattering, molecular oxygen absorption, and ozone absorption corresponding to London's nighttime ozone model.

Figure 15. Transmission function for molecular oxygen absorption corresponding to Colegrove, et al., average molecular oxygen profile.

Figure 16. U-V stellar spectra for various tangent ray heights during occultation with molecular scattering, molecular oxygen absorption, and ozone absorption.

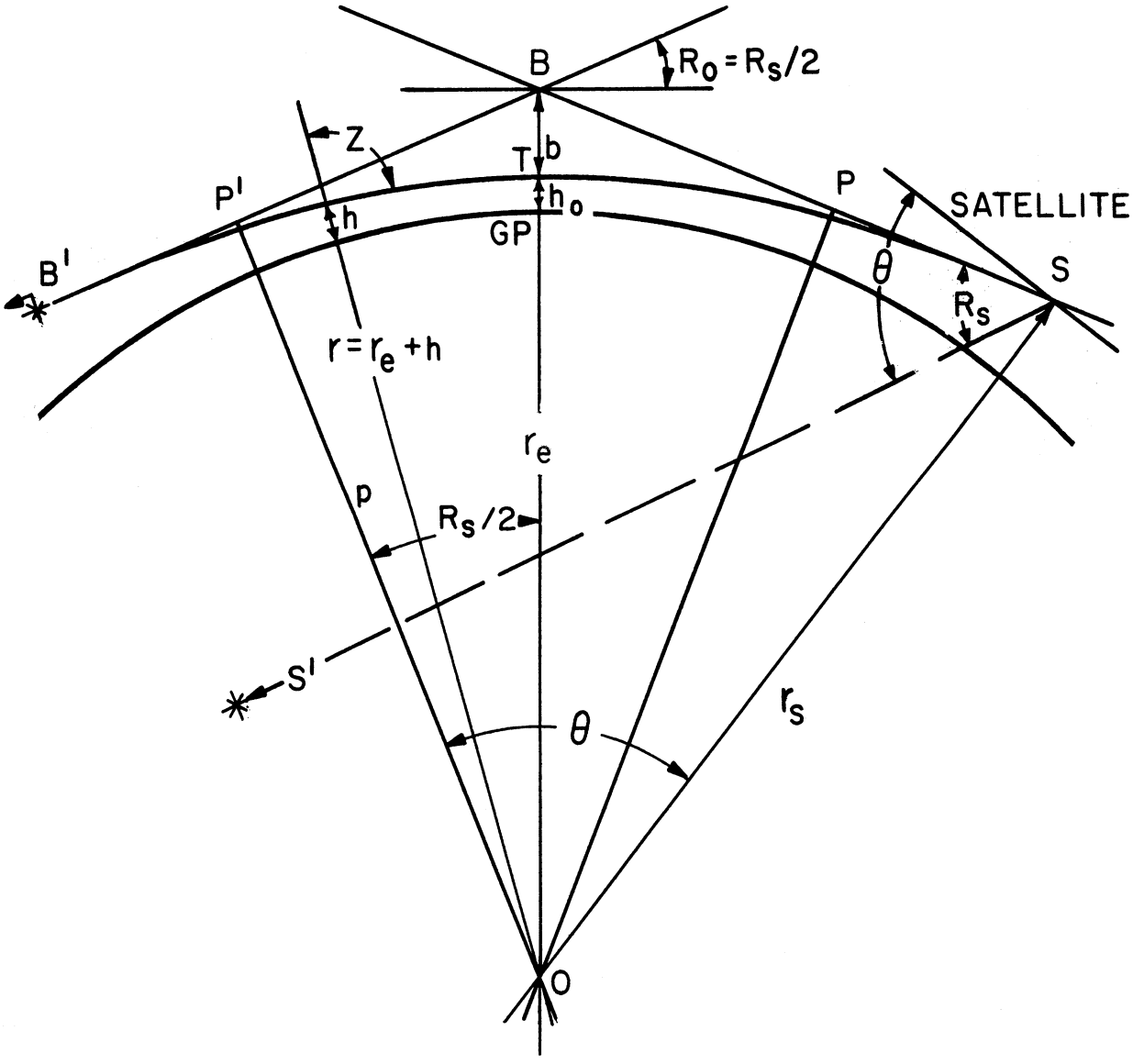
B
$R_0 = R_s/2$
Z
T
b
h_o
GP
P'
h
P
SATELLITE
B'
θ
S
R_s
$r = r_e + h$
r_e
p
$R_s/2$
S'
θ
r_s
O

Figure 1

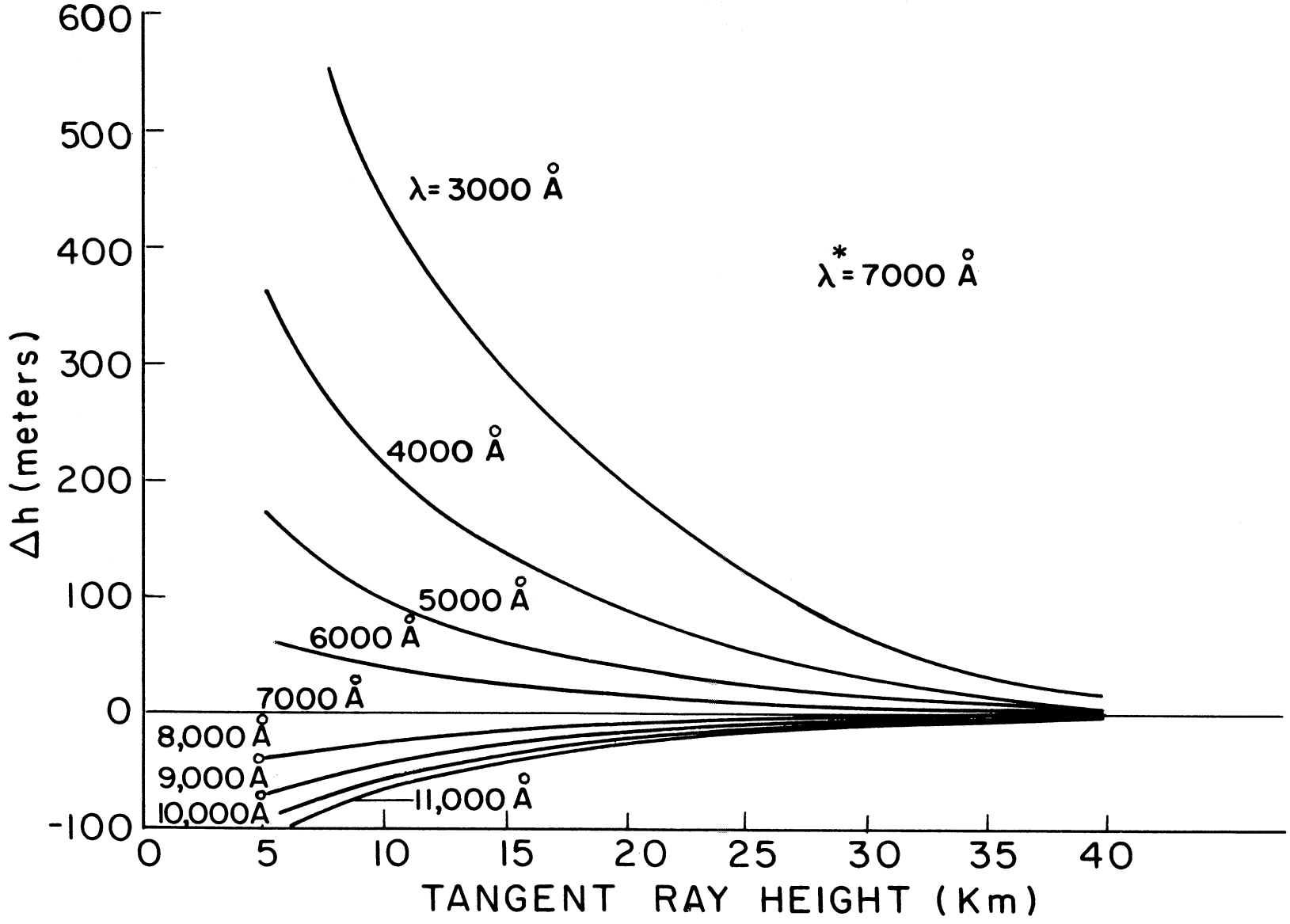
600
500
400
300
200
100
0
-100
Δh (meters)
λ= 3000 Å
λ*= 7000 Å
4000 Å
5000 Å
6000 Å
7000 Å
8,000 Å
9,000 Å
10,000 Å
11,000 Å
0
5
10
15
20
25
30
35
40
TANGENT RAY HEIGHT (Km)

Figure 2

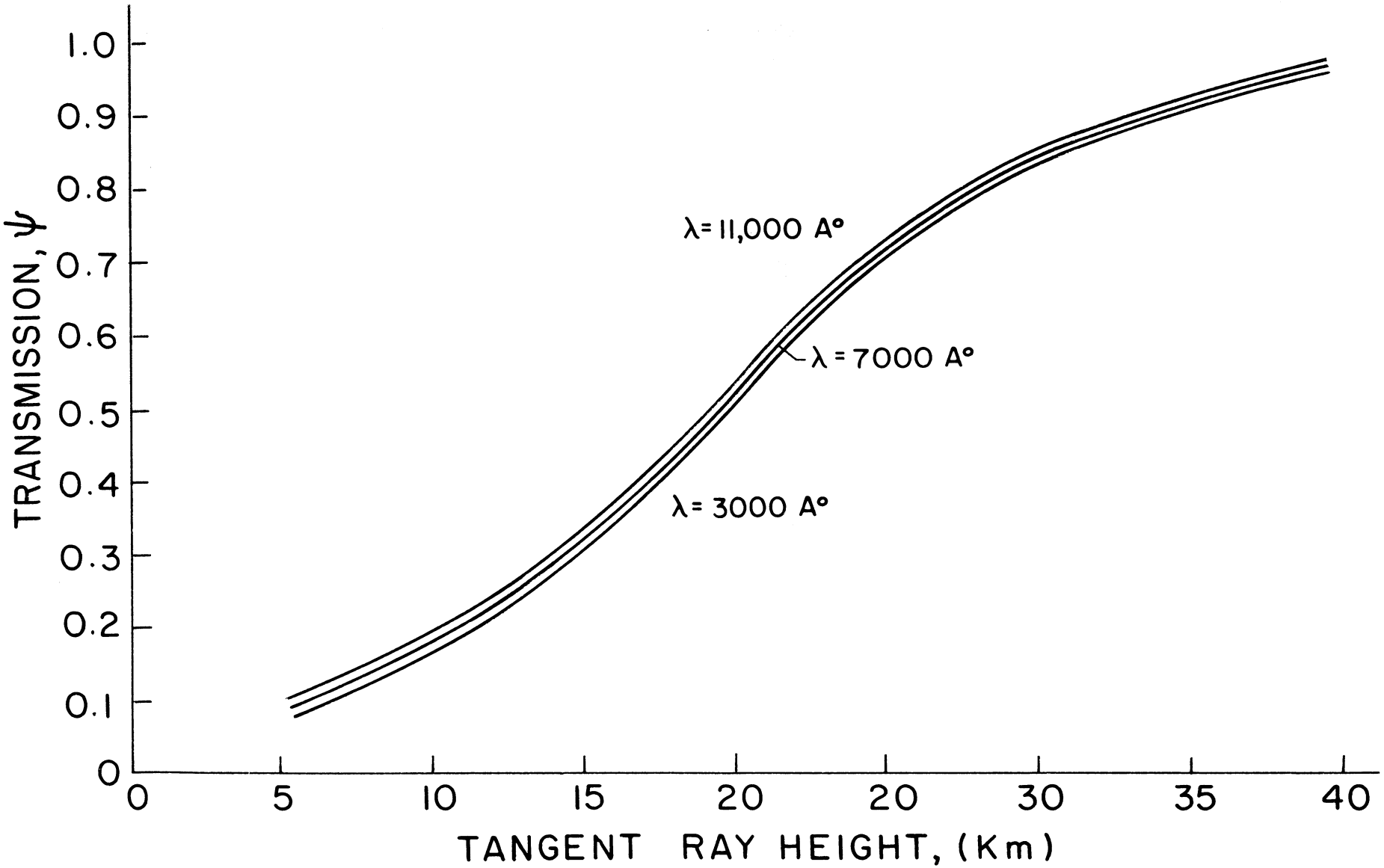
TRANSMISSION, ψ
1.0
0.9
0.8
0.7
0.6
0.5
0.4
0.3
0.2
0.1
0
λ= 11,000 A°
λ = 7000 A°
λ = 3000 A°
0
5
10
15
20
20
30
35
40
TANGENT RAY HEIGHT, (Km)

Figure 3

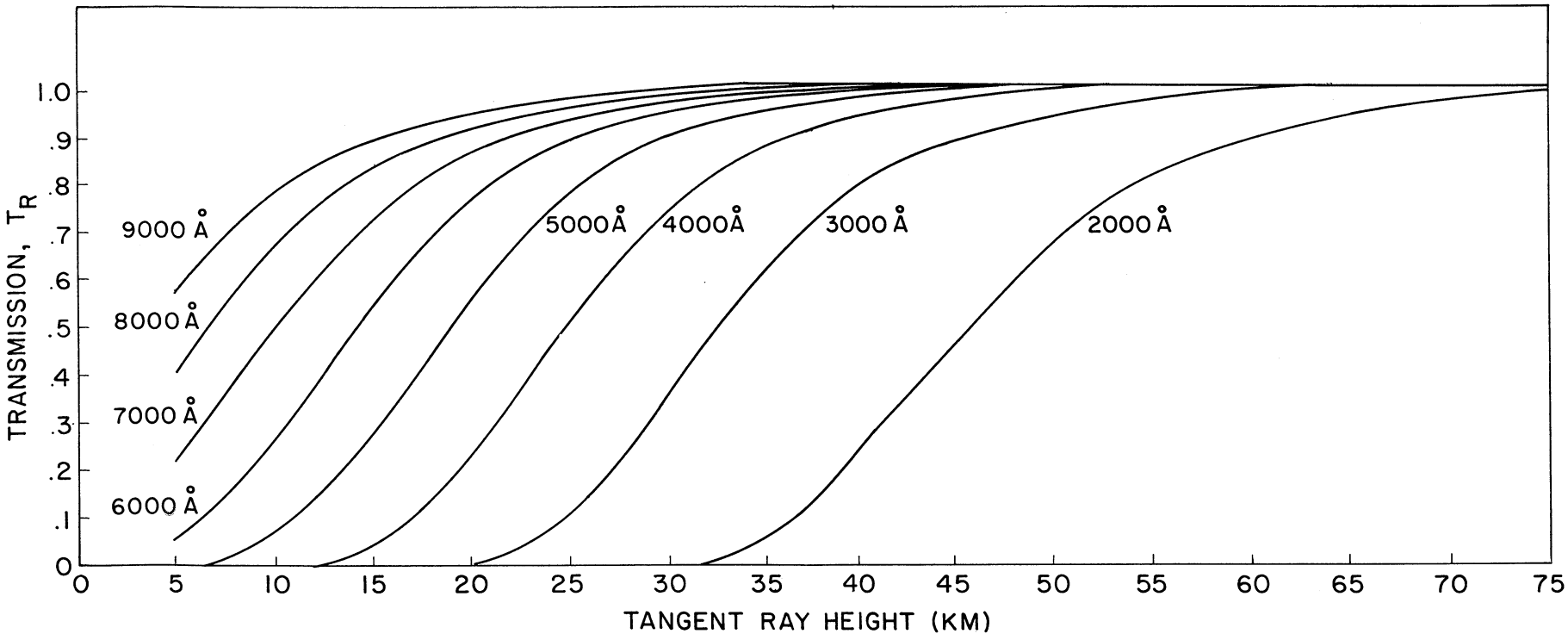
TRANSMISSION, T_R
1.0
.9
.8
.7
.6
.5
.4
.3
.2
.1
0
9000 Å
8000 Å
7000 Å
6000 Å
5000Å
4000Å
3000 Å
2000 Å
0
5
10
15
20
25
30
35
40
45
50
55
60
65
70
75
TANGENT RAY HEIGHT (KM)

Figure 4

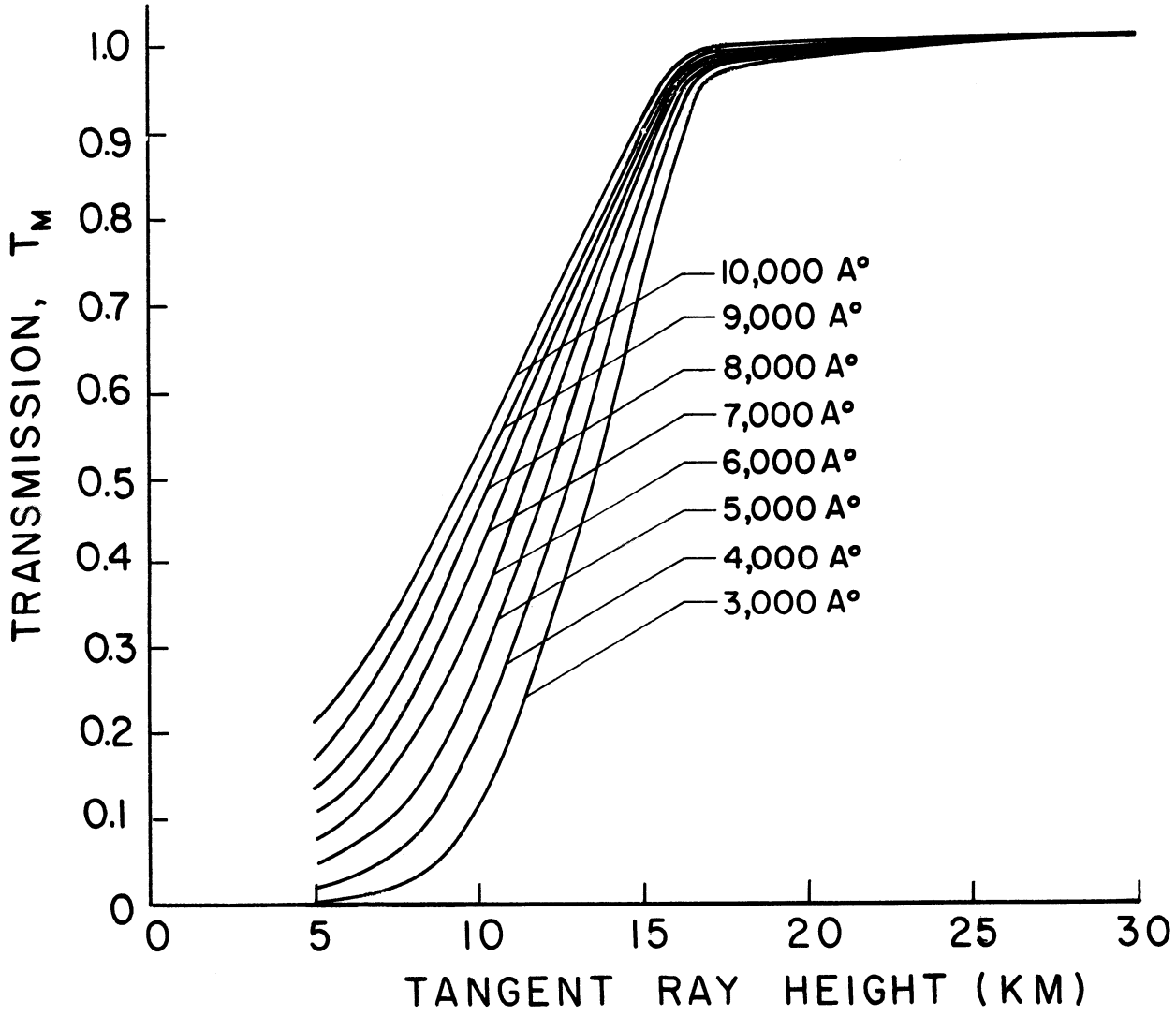
TRANSMISSION, T_M
1.0
0.9
0.8
0.7
0.6
0.5
0.4
0.3
0.2
0.1
0
0
5
10
15
20
25
30
TANGENT RAY HEIGHT (KM)
10,000 A°
9,000 A°
8,000 A°
7,000 A°
6,000 A°
5,000 A°
4,000 A°
3,000 A°

Figure 5

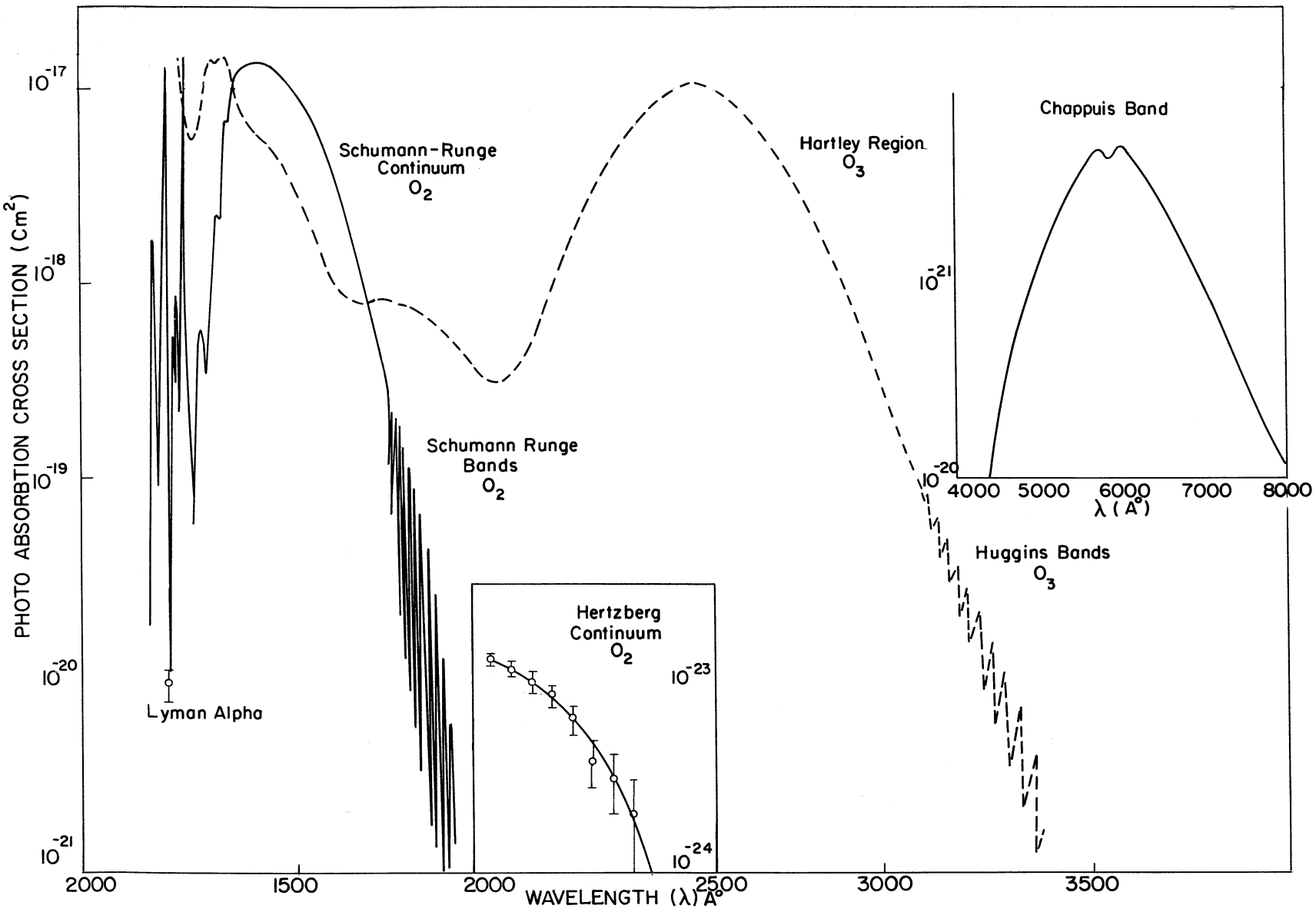
PHOTO ABSORBTION CROSS SECTION (Cm²)
10⁻¹⁷
10⁻¹⁸
10⁻¹⁹
10⁻²⁰
10⁻²¹
Schumann-Runge Continuum O₂
Hartley Region O₃
Chappuis Band
10⁻²¹
10⁻²⁰
4000 5000 6000 7000 8000
λ (A°)
Schumann Runge Bands O₂
Huggins Bands O₃
Hertzberg Continuum O₂
10⁻²³
10⁻²⁴
Lyman Alpha
2000 1500 2000 2500 3000 3500
WAVELENGTH (λ) A°

Figure 6

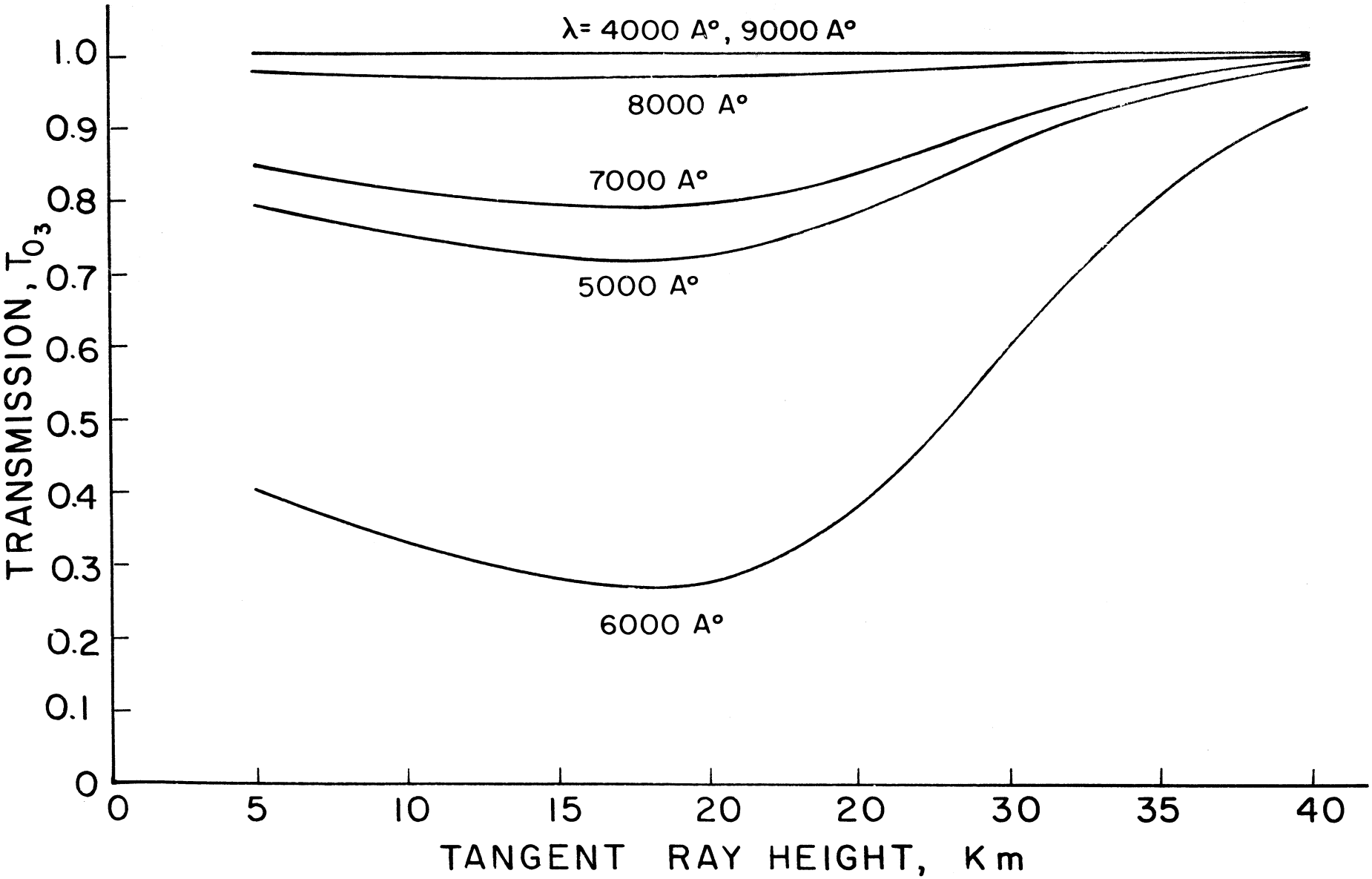
λ= 4000 A°, 9000 A°
8000 A°
7000 A°
5000 A°
6000 A°
TRANSMISSION, T_{O_3}
1.0
0.9
0.8
0.7
0.6
0.5
0.4
0.3
0.2
0.1
0
0
5
10
15
20
20
30
35
40
TANGENT RAY HEIGHT, Km

Figure 7

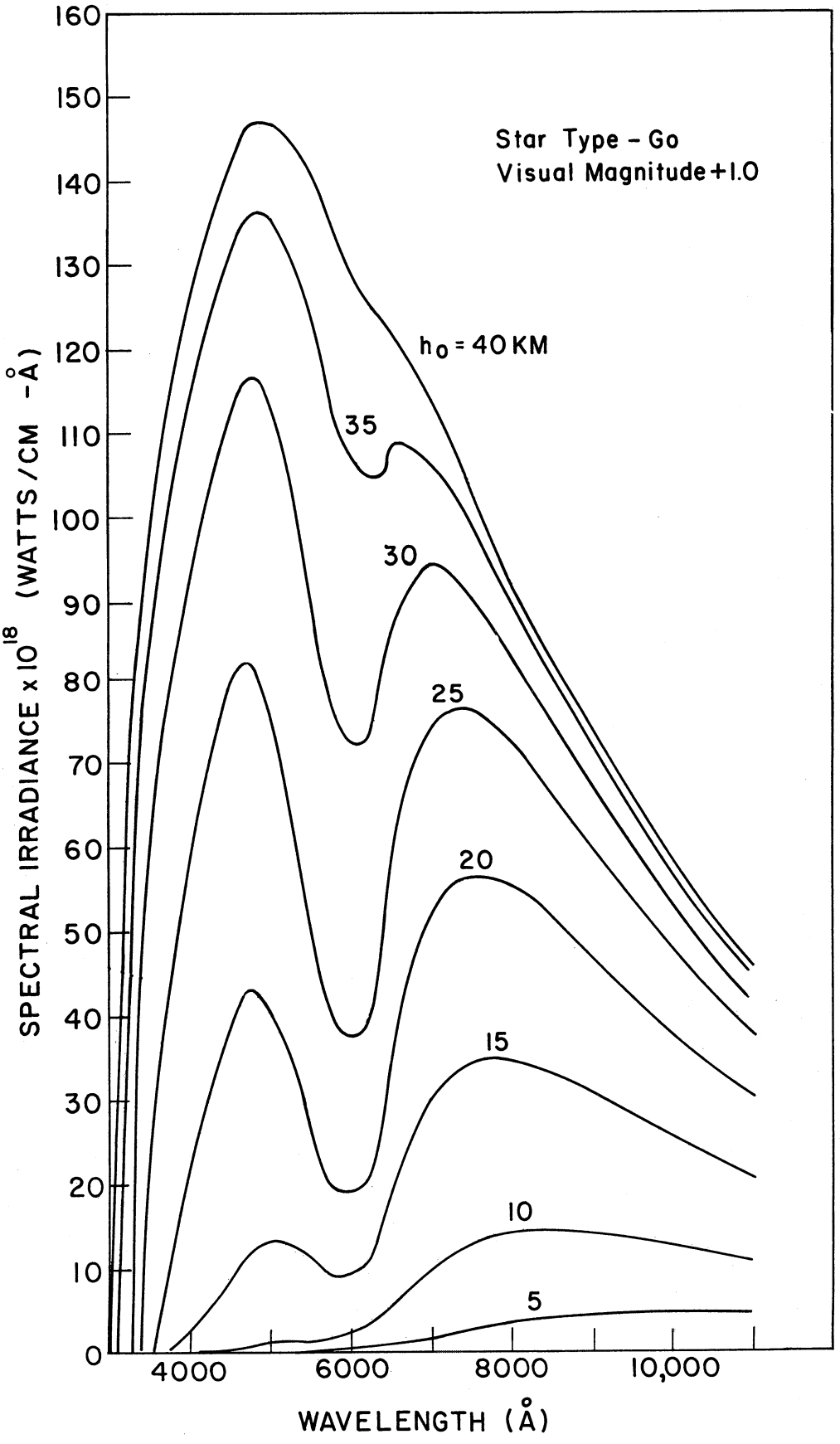
Star Type - Go
Visual Magnitude +1.0
h_o = 40 KM
35
30
25
20
15
10
5
SPECTRAL IRRADIANCE x 10^{18} (WATTS/CM - Å)
WAVELENGTH (Å)
0
10
20
30
40
50
60
70
80
90
100
110
120
130
140
150
160
4000
6000
8000
10,000

Figure 8

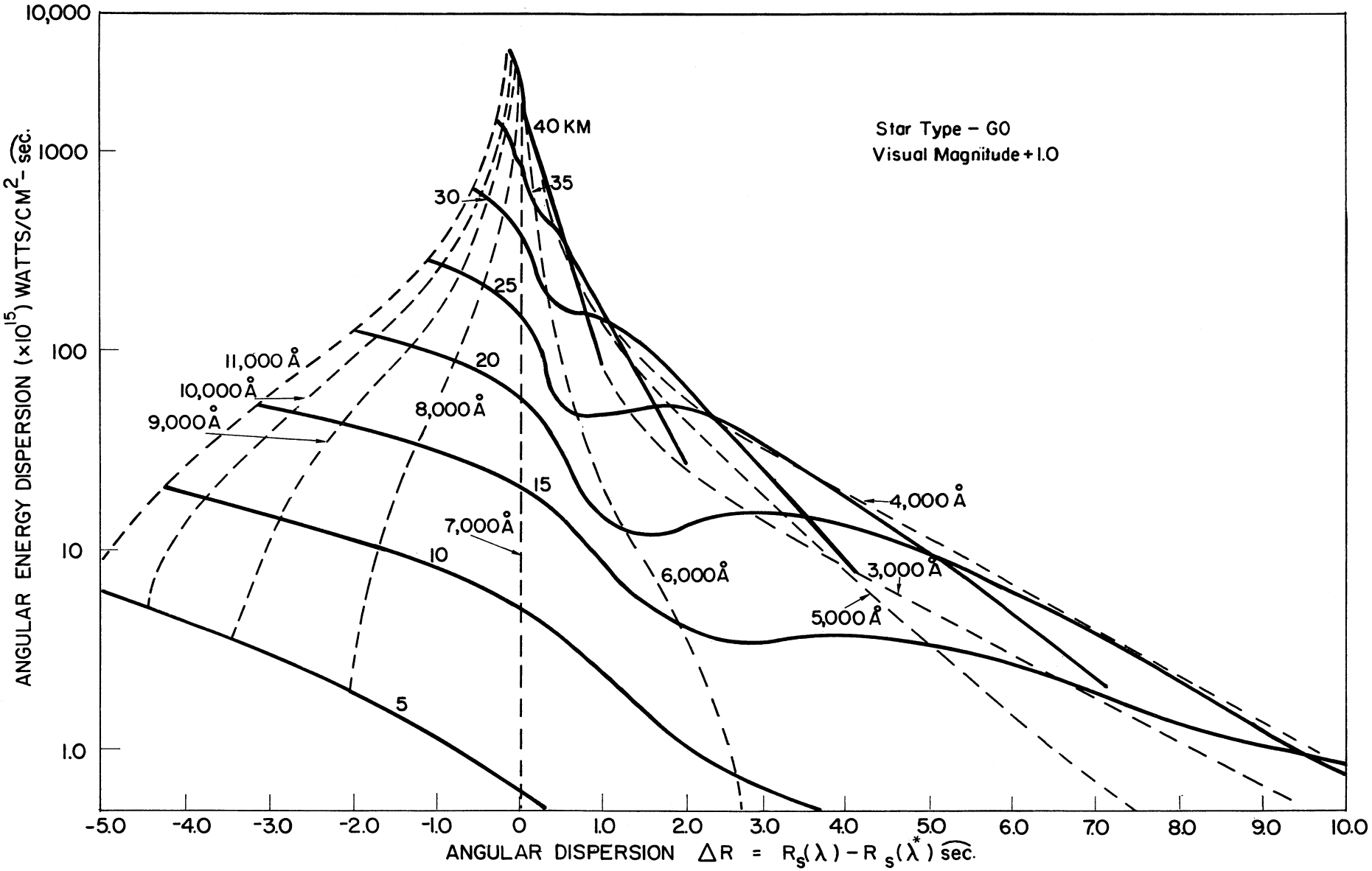
10,000
1000
100
10
1.0
ANGULAR ENERGY DISPERSION (×10^15) WATTS/CM^2 - sec.
Star Type – G0
Visual Magnitude + 1.0
40 KM
35
30
25
20
15
10
5
11,000 Å
10,000 Å
9,000 Å
8,000 Å
7,000 Å
6,000 Å
5,000 Å
4,000 Å
3,000 Å
-5.0
-4.0
-3.0
-2.0
-1.0
0
1.0
2.0
3.0
4.0
5.0
6.0
7.0
8.0
9.0
10.0
ANGULAR DISPERSION ΔR = R_s(λ) – R_s(λ*) sec.

Figure 9

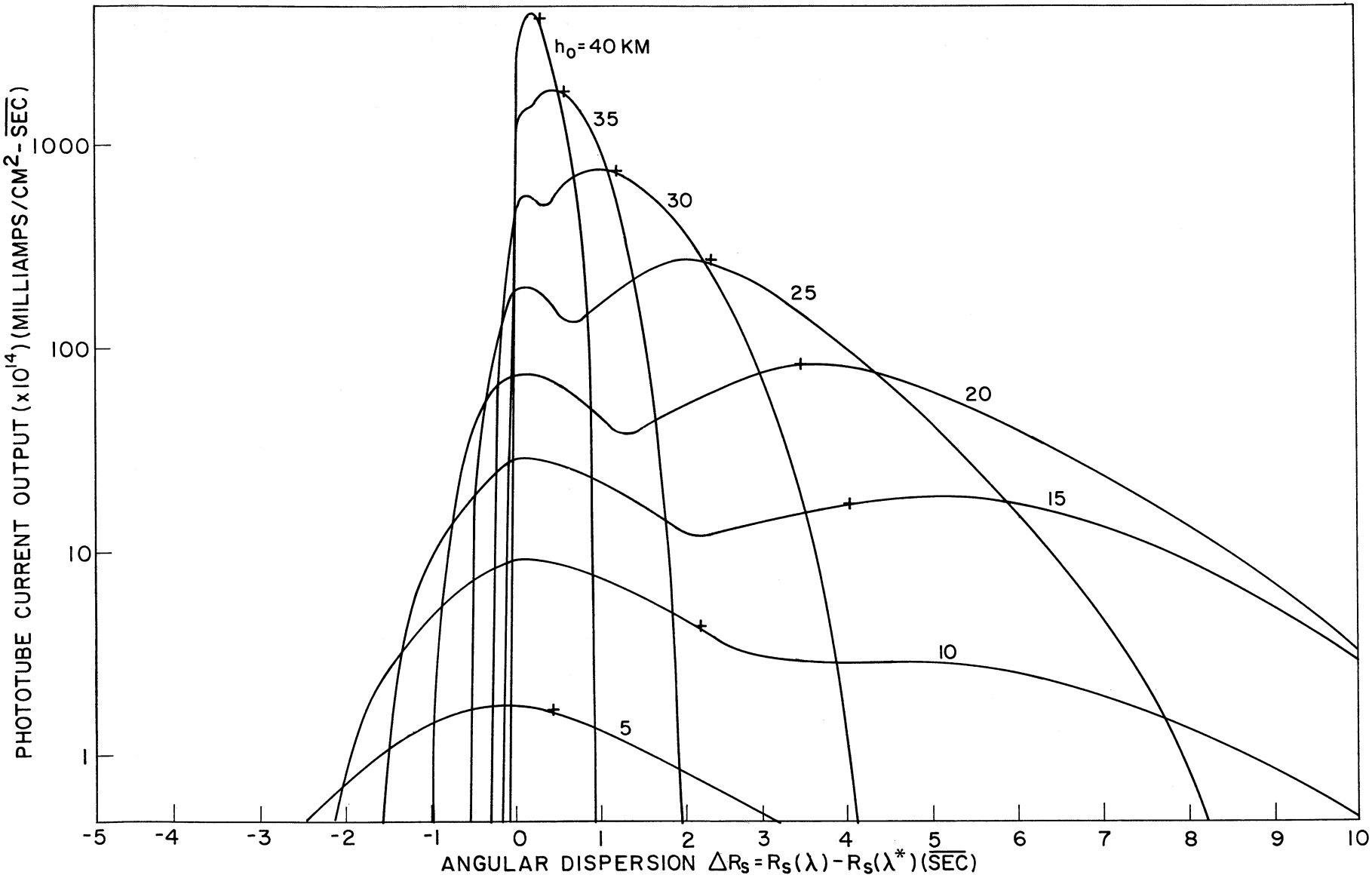
PHOTOTUBE CURRENT OUTPUT (x10^14) (MILLIAMPS/CM^2-SEC)
1000
100
10
1
h0=40 KM
35
30
25
20
15
10
5
-5
-4
-3
-2
-1
0
1
2
3
4
5
6
7
8
9
10
ANGULAR DISPERSION ΔRs=Rs(λ)-Rs(λ*)(SEC)

Figure 10

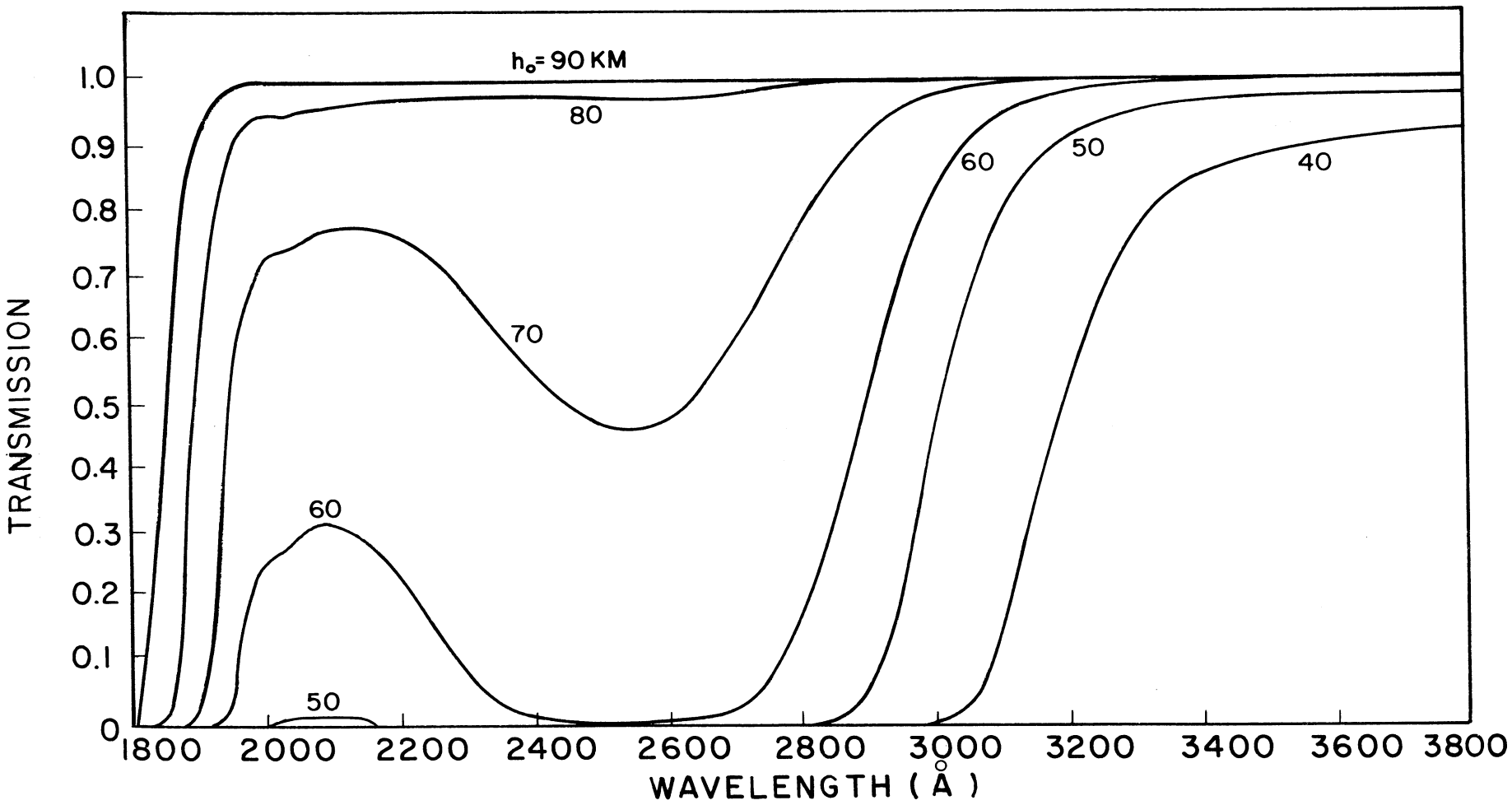
h_o= 90 KM
80
60
50
40
70
60
50
TRANSMISSION
1.0
0.9
0.8
0.7
0.6
0.5
0.4
0.3
0.2
0.1
0
1800
2000
2200
2400
2600
2800
3000
3200
3400
3600
3800
WAVELENGTH (Å)

Figure 11

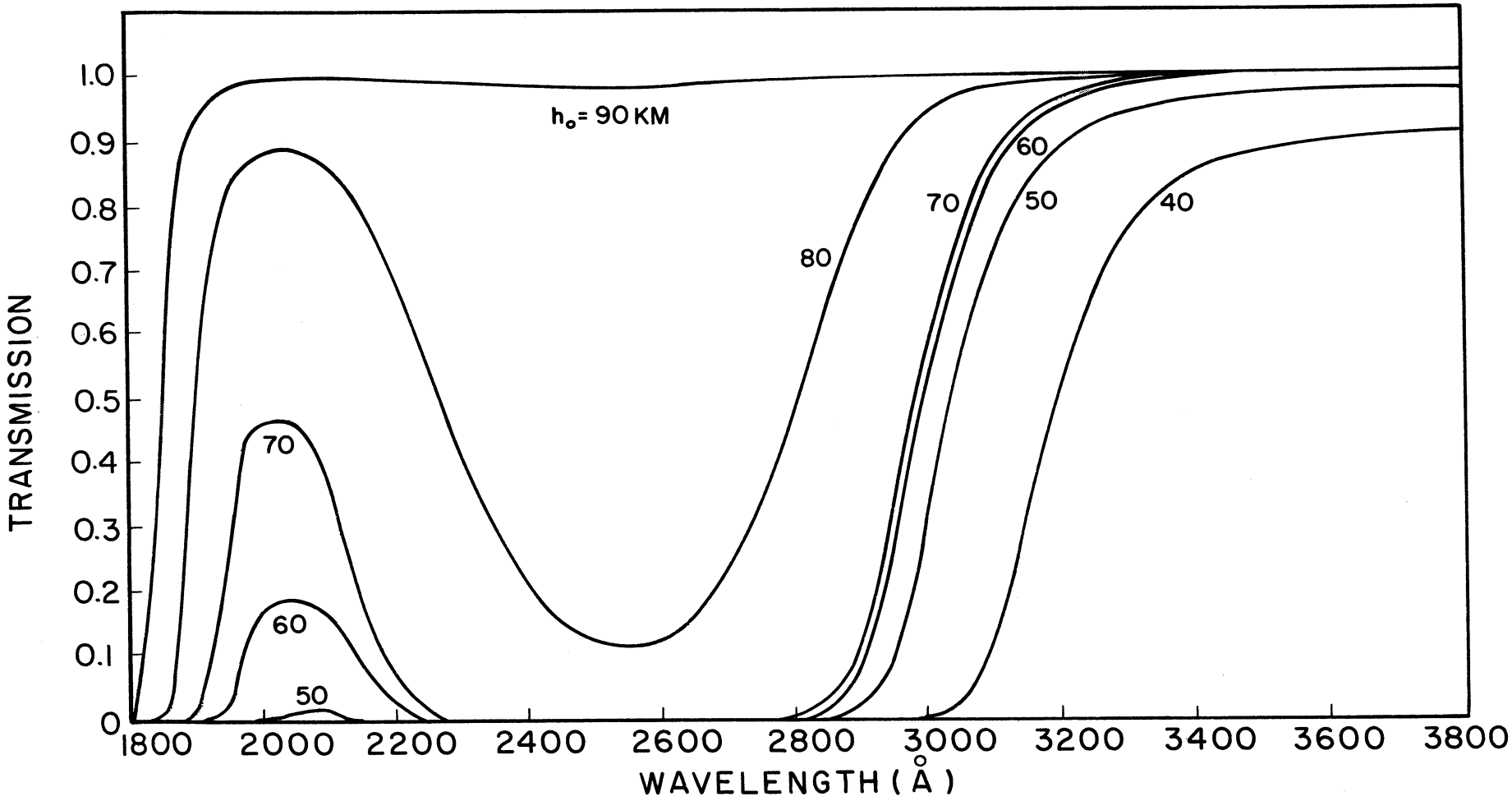
TRANSMISSION
1.0
0.9
0.8
0.7
0.6
0.5
0.4
0.3
0.2
0.1
0
h_o= 90 KM
80
70
60
50
40
70
60
50
1800
2000
2200
2400
2600
2800
3000
3200
3400
3600
3800
WAVELENGTH (Å)

Figure 12

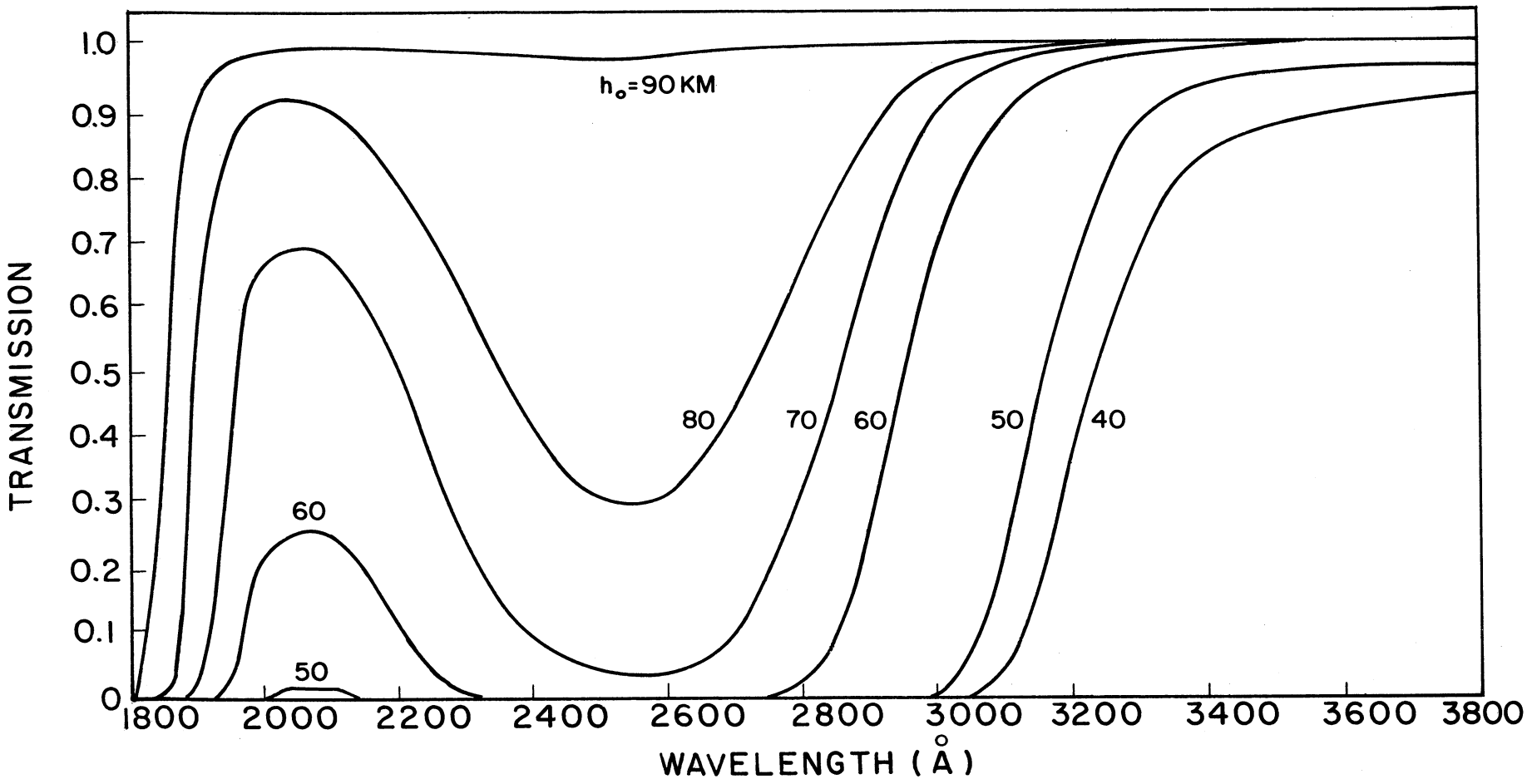
TRANSMISSION
1.0
0.9
0.8
0.7
0.6
0.5
0.4
0.3
0.2
0.1
0
h_o=90 KM
80
70
60
50
40
60
50
1800
2000
2200
2400
2600
2800
3000
3200
3400
3600
3800
WAVELENGTH (Å)

Figure 13

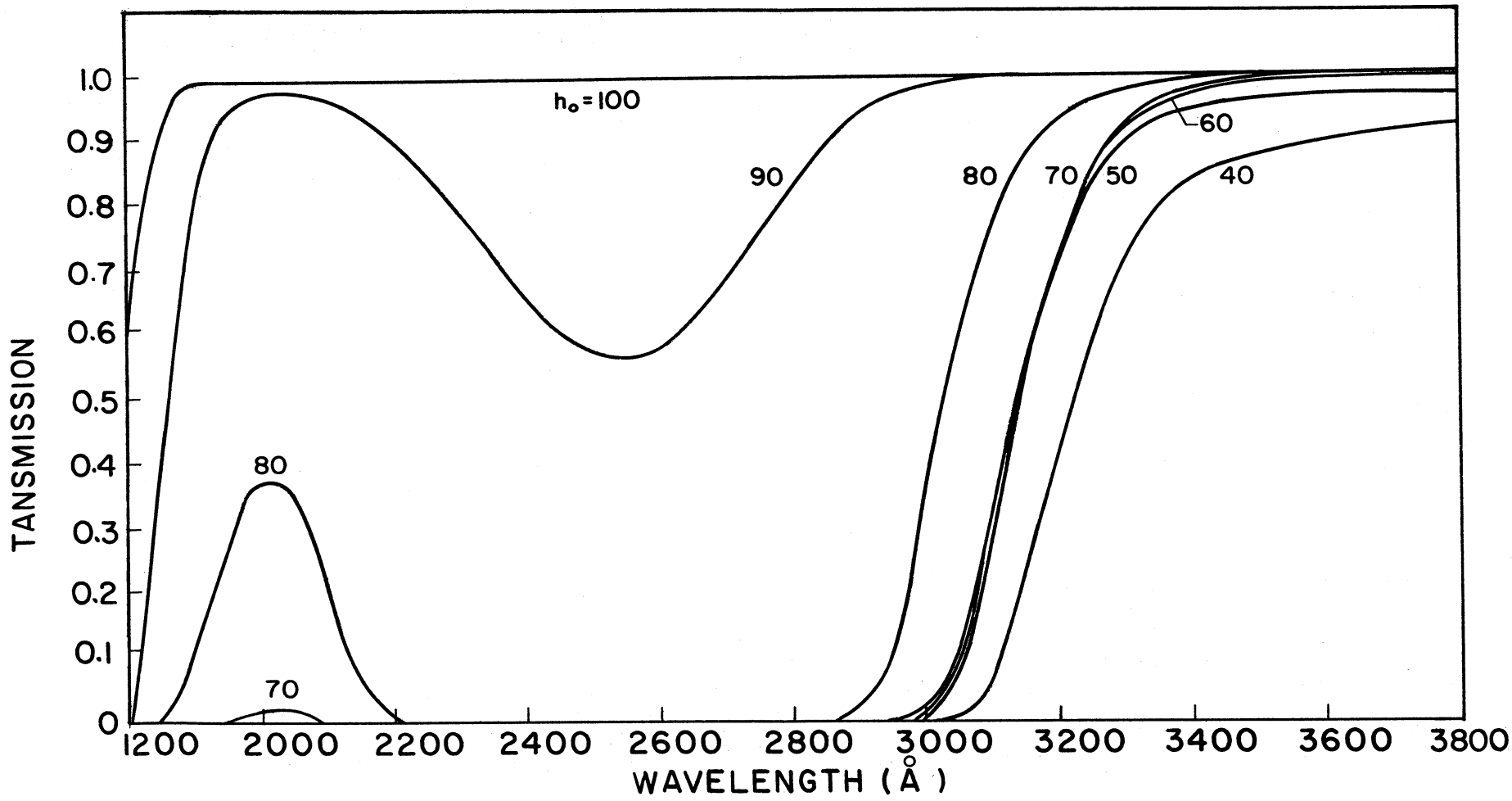
TANSMISSION
1.0
0.9
0.8
0.7
0.6
0.5
0.4
0.3
0.2
0.1
0
h_o = 100
90
80
70
50
60
40
80
70
1200
2000
2200
2400
2600
2800
3000
3200
3400
3600
3800
WAVELENGTH (Å)

Figure 14

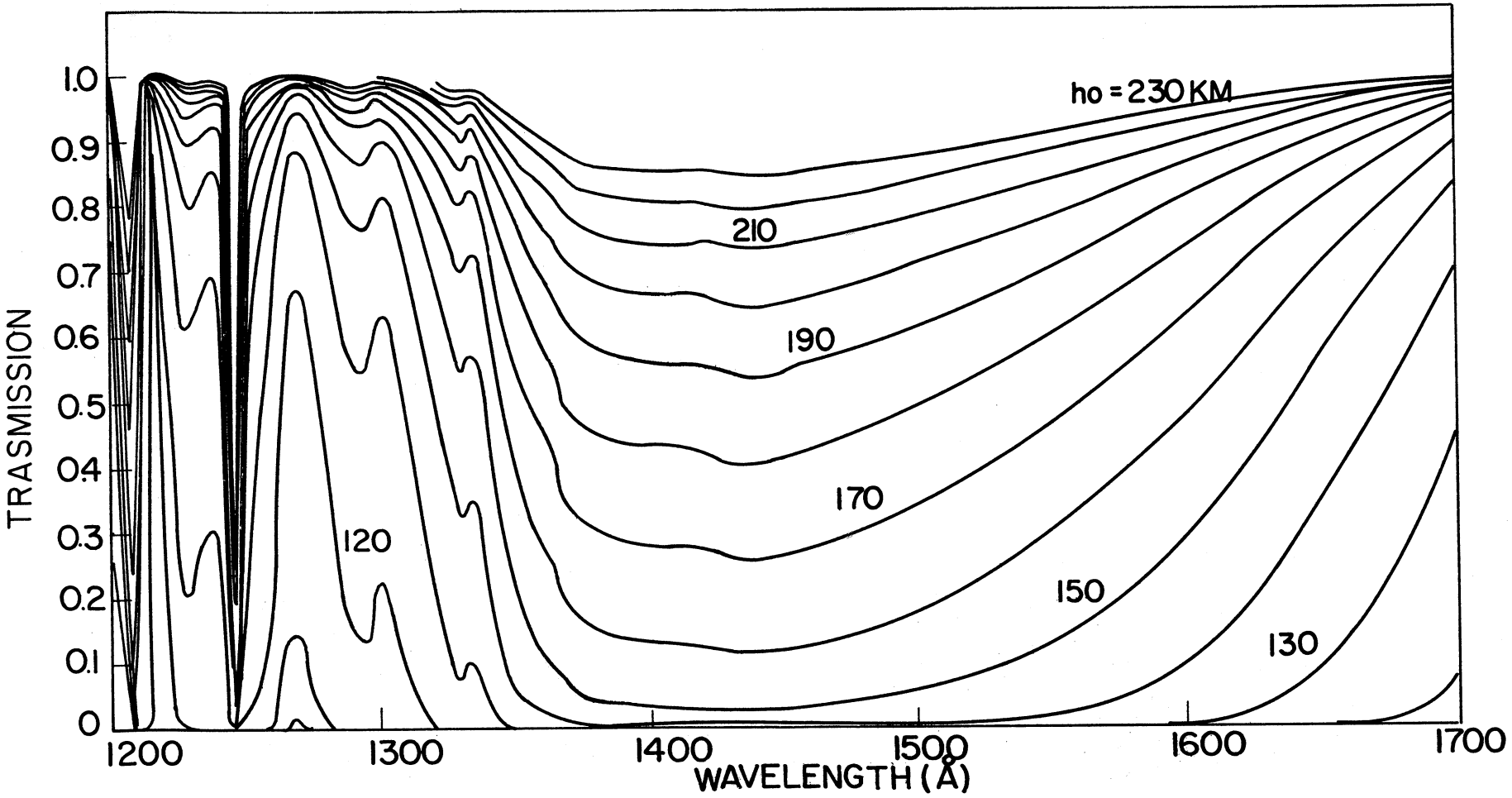
TRASMISSION
1.0
0.9
0.8
0.7
0.6
0.5
0.4
0.3
0.2
0.1
0
1200
1300
1400
1500
1600
1700
WAVELENGTH (Å)
ho = 230 KM
210
190
170
150
130
120

Figure 15

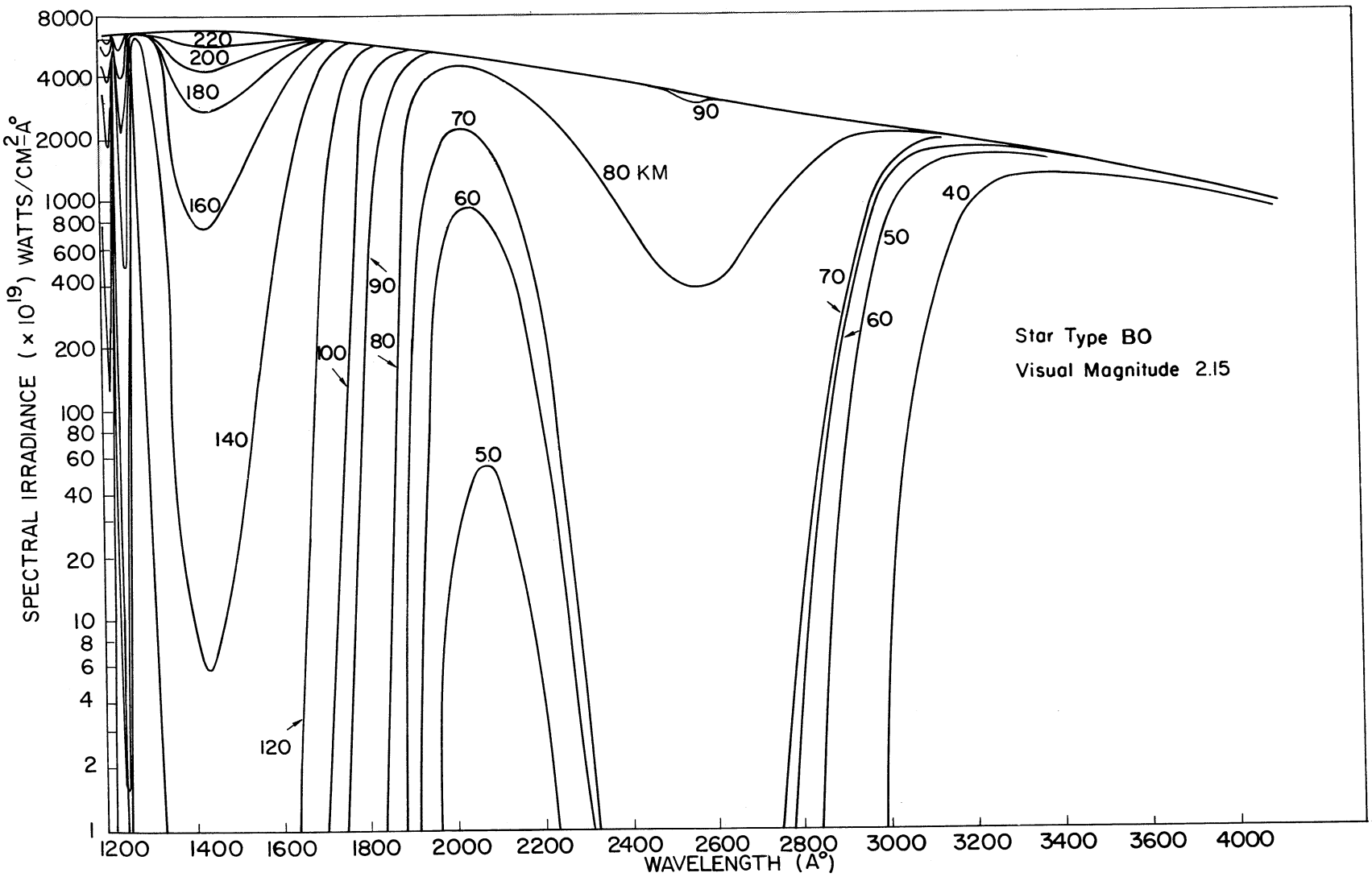
SPECTRAL IRRADIANCE (x 10^19) WATTS/CM^2-A°
WAVELENGTH (A°)
8000
4000
2000
1000
800
600
400
200
100
80
60
40
20
10
8
6
4
2
1
1200
1400
1600
1800
2000
2200
2400
2600
2800
3000
3200
3400
3600
4000
220
200
180
160
140
120
100
90
80
70
60
50
40
90
80 KM
70
60
50
40
Star Type BO
Visual Magnitude 2.15

Figure 16